Microchemical Journal 193 (2023) 109060

Contents lists available at ScienceDirect

Microchemical Journal

journal homepage: www.elsevier.com/locate/microc

Fabrication of molecularly imprinted electrochemical sensors for sensitive codeine detection

Merve Yence [a,b], Ahmet Cetinkaya [a,b], Mehmet Emin Çorman [c], Lokman Uzun [d], Mehmet Gokhan Caglayan [a,*], Sibel A. Ozkan [a,*]

[a] Faculty of Pharmacy, Department of Analytical Chemistry, Ankara University, 06560, Turkey
[b] Ankara University, Graduate School of Health Sciences, 06110, Turkey
[c] Gülhane Faculty of Pharmacy, Department of Biochemistry, University of Health Sciences, 06018, Turkey
[d] Faculty of Science, Department of Chemistry, Hacettepe University, 06800, Turkey

ARTICLE INFO

Keywords:
Codeine
Molecularly imprinted polymer
Electrochemical determination
Photopolymerization

ABSTRACT

Codeine (COD) is a natural opiate alkaloid obtained from hashish or prepared by methylation from morphine, widely used as an analgesic, antitussive, and antidiarrheal drug. A sensitive and selective electrochemical sensor based on molecular imprinting polymer (MIP) was developed to detect COD in tablet form and biological fluid samples. The polymeric thin film on the glassy carbon electrode (GCE) surface was formed using template molecule COD, a functional monomer based on amino acid N-methacryloyl-L-tryptophan (MA-Trp), basic monomer 2-hydroxyethyl methacrylate (HEMA), cross-linker ethylene glycol dimethacrylate (EGDMA), and the pore-making sacrificial material zinc oxide (ZnO). The developed MIP-based electrochemical sensor (MA-Trp@MIP/GCE) was characterized by scanning electron microscopy (SEM), Fourier-transform infrared spectroscopy (FT-IR), cyclic voltammetry (CV), and electrochemical impedance spectroscopy (EIS) methods. The electrochemical properties of the sensor were examined using differential pulse voltammetry (DPV). Under optimum experimental conditions, the dynamic linear range of the developed sensor was calculated as 0.1–1.0 pM and the detection limit of 0.0150 pM. The current electrochemical sensor technique also demonstrated outstanding recovery in human urine, synthetic serum samples, and tablet form, with relatively high recoveries of 98.5%, 101.4%, and 101.5%, respectively. Moreover, the MA-Trp@MIP/GCE sensor exhibited good reproducibility, repeatability, stability, and fast response time for the electrochemical analysis of COD. The presented sensor successfully determined COD in tablet and biological fluid samples.

1. Introduction

Codeine (COD) is one of the most frequently used opiates and is an anti-tussive, antidiarrheal, and analgesic drug [1]. French chemist Pierre-Jean Robiquet first isolated it in 1832, and it can be extracted directly from opium, one of the earliest pharmaceutical substances ever discovered [2]. In addition, it is often made for medical usage by methylation of morphine to produce a fine-needle-shaped white crystal or powder [3]. The cytochrome P450 enzyme (CYP) 2D6 converts ten percent of codeine to morphine, and this enzyme's inhibitors can reduce or even eliminate the effects of the codeine [2,4]. Codeine and its metabolite morphine are naturally occurring opium alkaloids and have analgesic effects in mild to moderate pain management [5,6]. Even though they are thought to be essential for pain management, there are well-known risks associated with an opioid prescription, such as misuse, dependence, and overdose deaths [5]. About 40% of users fit the criteria for codeine dependence, and using products with codeine is significantly linked to endogenous depression, creating another issue with dual diagnoses [7]. Besides these risks, there are other adverse effects on human health, especially on the reproductive system. Recently, the effects of codeine on female reproductive health were assessed by Akhigbe et al. [8], offering some of the first proof of the negative consequences of prolonged codeine usage on female sexual function, ovarian steroidogenesis, and folliculogenesis.

Since COD is not only an active pharmaceutical ingredient but also a forensic analyte, various analytical methods have been developed for its detection in different sample matrices. Codeine can be screened in different biological matrices such as urine and blood, for up to three

* Corresponding authors.
E-mail addresses: gcaglayan@ankara.edu.tr (M.G. Caglayan), sibel.ozkan@pharmacy.ankara.edu.tr (S.A. Ozkan).

https://doi.org/10.1016/j.microc.2023.109060
Received 24 December 2022; Received in revised form 2 April 2023; Accepted 30 June 2023
Available online 6 July 2023
0026-265X/© 2023 Elsevier B.V. All rights reserved.

days [9] and cut-off values for a codeine screening test are set from 300 ng/mL to 2000 ng/mL in different countries [10]. In this regard, a variety of analytical methods, such as high-performance liquid chromatography [11–13], gas chromatography-mass spectrometry [14], colorimetric detection [15], and surface-enhanced Raman spectroscopy [16] have been widely used. However, chromatographic-based methods require expert personnel, high-cost analytical devices and their pieces of equipment, complicated pre-treatment experimental procedures, and toxic chemicals [5,17]. Colorimetric testing kits such as Marquis, Froehde's, and Mecke's reagents are based on the colorimetric readout. Although they are suitable for on-site analysis and easy to implement, they give similar colors to different opioids. Hence, it is challenging to acquire reliable results and exhibit selectivity. Electrochemical sensors offer a variety of advantages over these methods in terms of good sensitivity, easy experimental analysis preparation, miniaturization and portability of devices, usage of green solvents and materials, also short analysis time. Especially, molecularly imprinted polymers in combination with electrochemical sensors (MIPs) provide more sensitivity and selectivity. A specific template molecule, which can be selectively recognized among other elements found in the complex sample matrix, is used to synthesize MIP. This technique has numerous benefits, such as specific recognition, a particular affinity for the template, high binding capacity, and a broad applicability [18,19]. MIPs thought to be a flexible and promising method that can identify both biological and chemical compounds, including drugs [20–22], biomedical markers and pathogens [23], amino acids [24], and pollutants [25,26]. MIPs-based electrochemical sensors improve specificity, especially with the design of particular functional monomers. Selecting particular monomers forming a complex structure with the template is essential for a stable polymer matrix. There are several studies on the design and synthesis of functional monomers [21,27]. Çorman et al. suggested a nucleobase-based functional monomer, thymine methacrylate (ThyM) to build a prepolymer complex with the drug ruxolitinib that has an adenine structure. Since adenine and thymine have strong hydrogen bonding properties, drugs and monomer form well-built molecularly imprinted material [27]. Çetinkaya and colleagues has chosen a functional monomer *ortho*-phenylenediamine (*o*-PD) depend on computational studies which compare interaction energies between drug leflunomide and monomer to develop a more stable sensor [22]. Generally, photopolymerization and thermal polymerization are common techniques for synthesizing MIPs. In fact, photopolymerization has gained significant popularity over the past decade and is now frequently the preferred strategy. The reasons behind it can be explained by two primary arguments. Firstly, radicals are generated with the help of light that requires low temperature which leads protection of sensitive interactions. Secondly, the radical production can be instantly switched on or off by automatically turning on or off the light source. These help to control polymerization process and minimize side products [28].

In the present work, a molecularly imprinted electrochemical sensor (MA-Trp@MIP/GCE) was developed using a functional monomer based on amino acid, N-methacryloyl-L-tryptophan (MA-Trp), hydroxyethyl methacrylate (HEMA), ethylene glycol dimethacrylate (EGDMA), and pore-making sacrificial material zinc oxide (ZnO), 2-hydroxy-2-methyl propiophenone as a photoinitiator in the presence of COD with photopolymerization on the glassy carbon electrode (GCE) for the first time. Firstly, MA-Trp was synthesized by one step and unchallenging method. As a pretreatment step COD was adsorbed on ZnO particles, then MA-Trp copolymerized with HEMA in the company of EGDMA as the cross-linker. The purpose of using ZnO nanoparticles is to create a controlled surface imprinting procedure during polymerization and to form porous structures after removal. Therefore, ZnO nanoparticles increase the pore structure, provide oriented recognition sites and improve the mass transfer properties [29,30]. The prepared (MA-Trp@MIP/GCE) sensor was characterized with Fourier transform infrared (FT-IR) spectroscopy, scanning electron microscopy (SEM), cyclic voltammetry, and impedance spectroscopy technique. This proposed method detected COD in the pharmaceutical dosage form, urine, and synthetic human serum samples. To the best of our knowledge, this is the first MIPs-based electrochemical sensor study for the detection of COD.

2. Experimental

2.1. Reagents and apparatus

COD powder is a gift sample from the Soil Products Office in Turkiye, and apranax plus® tablets were provided from the pharmacy. The mixture of 5 mM $[Fe(CN)_6]^{3-/4-}$ (1:1) in 0.1 M potassium chloride (KCl) solution was prepared using tetra potassium hexacyanoferrate $[K_4Fe(CN)_6]$ and tripotassium hexacyanoferrate $[K_3Fe(CN)_6]$ those provided from Merck. Hydroxyethyl methacrylate (HEMA), ethylene glycol dimethacrylate (EGDMA), 2-hydroxy-2-methyl propiophenone, acetic acid, methanol (99.8%), zinc oxide (ZnO), and commercial human serum from were purchased from Sigma-Aldrich. ZnO particles (1 mg) were dispersed in 10 mL of COD solution in methanol (0.1 mg/mL) and subsequently sonicated for 15 min before utilizing a pore-making agent and stored at room temperature. 1.0 mM stock solution of MA-Trp was prepared in 2 mL MeOH and stored at + 4 °C.

PalmSens Potensiostat (Netherlands) was used to perform all voltammetric measurements, including cyclic voltammetry (CV) and differential pulse voltammetry (DPV). It was connected to an electrochemical cell of 5 mL with a three-electrode system: an Ag/AgCl electrode (reference electrode), a platinum wire (auxiliary electrode), and a glassy carbon electrode (working electrode, 3 mm diameter, BASi). The AUTOLAB (Netherlands) potentiostat/galvanostat was used to conduct electrochemical impedance spectroscopy (EIS) studies (NOVA 2.1.5 software).

A precise balance made by Ohaus Instruments (Shanghai, China) was used for the weighing. The methods for removing and rebinding were carried out in a Thermo-Shaker (Biosan TS-100). Fourier transform infrared (FTIR) spectrum in the wave number range of 4000 and 600 cm^{-1} was recorded with the ATR-FTIR 8000 series in Shimadzu, Japan. The morphological characterization of the sensor surface was performed using scanning electron microscopy (SEM, TESCAN GAIA 3, Brno-Kohoutovice, Czech Republic).

2.2. Synthesis of functional monomer

The amino acid-based functional monomer, N-methacryloyl-L tryptophan (MA-Trp), was synthesized according to previous literature shown in Fig. 1A and its possible interaction with COD shown in Fig. 1B [31]. L- Tryptophan (5.52 mmol) was dissolved in an aqueous solution of NaOH (1.0 M). A solution of MA-Bt (5.52 mmol) in 4-dioxane (25 mL) was slowly added into the L- tryptophan solution ambient. Following the completion of the reaction, 1,4-dioxane was vaporized in a vacuum. To remove the 1H-benzotriazole, the residue was diluted with water and extracted three times with ethyl acetate. Finally, water was removed by a rotary evaporator to give a yield MA-Trp monomer. ^{1}H NMR spectrum of MATrp was used to demonstrate the characteristic peaks from the groups in the monomer. ^{1}H NMR spectrum were shown in Fig. S1.

2.3. Preparation of the MIP and NIP-based electrodes with a polymeric film

Bare GCE was cleaned with methanol (MeOH) and deionized water solution (1:1, v/v) via sonication for 15 min. Secondly, the GCE was polished by alumina suspension, washed with ultrapure water, and dried at room temperature. The molecularly imprinted porous polymeric film was prepared as follows: 10 μL homogeneous solution of COD: ZnO (1:1 M ratio, 10 mL MeOH) was mixed with 30 μL of MA-Trp sonicated for 10 min. After, HEMA: EGDMA (5:1 v/v, 100 μL) was added and mixed for 10 min to form a stock solution. This stock solution, 10 μL was taken and

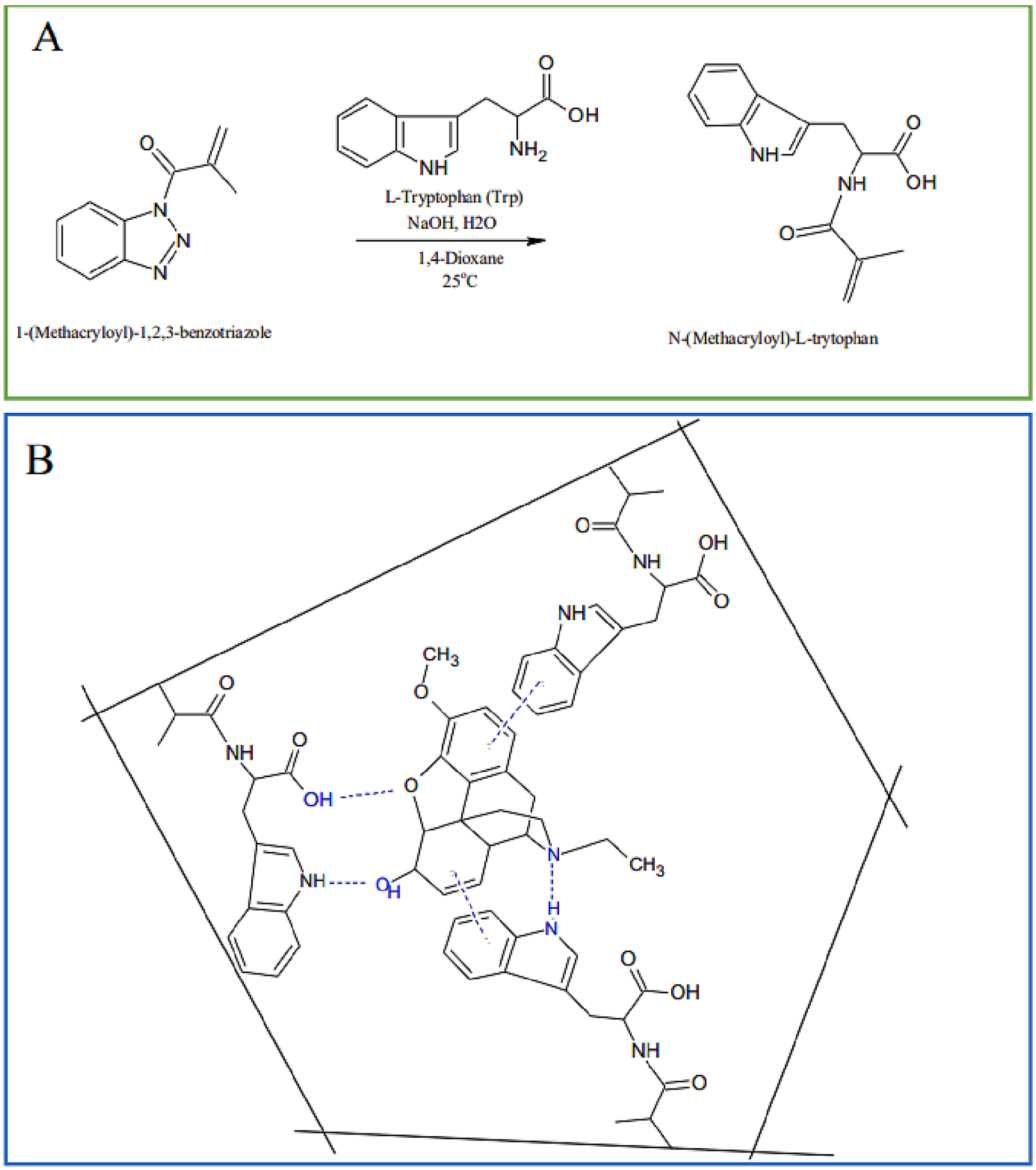


Fig. 1. A) The synthesis of MA-Trp B) Proposed interaction mechanism of MA-Trp and COD.

mixed with 1.0 μL 2-hydroxy-2-methyl propiophenone; then, the mixture was vortexed for 1 min. 0.5 μL of the mixture was dropped onto the electrode surface and polymerized under a UV lamp (365 nm, 100 W) for 5 min. To remove the ZnO particles, etching procedures were carried out by treating 0.1 M HCl solution and forming porous films. By rinsing with ethanol followed by washing with distilled water, the unreacted monomers were removed from the polymer. In this manner, MIP-based electrodes were constructed. For template extraction from the polymer matrix, the electrode was immersed in a 10 M acetic acid solution in a shaker (650 rpm, 25 °C) for 20 min. For rebinding of the template molecule, the electrode was incubated to a specific concentration of COD in a shaker (650 rpm, 25 °C) for 20 min.

Non-imprinted polymeric (NIP) based electrode constructed with the above polymeric film synthesis method without a template to assess imprinting effectiveness. The MIP-based sensor and the NIP-based sensor were compared. All electrochemical experiments were carried out indirectly with $[Fe(CN)_6]^{3-/4-}$ solution as a redox probe.

2.4. Tablet dosage form, serum, and urine sample applications

The mean of five tablets was weighed and pulverized for recovery experiments tablets. 1.0 mM COD tablet stock solution was prepared with pure methanol. The solution was sonicated, filtered, and centrifuged at 5000 rpm for 20 min. A certain amount was taken from the filtered solution and diluted in methanol then a calibration curve of COD from the tablet form was obtained. After that, the recovery study was applied by adding a known COD concentration to demonstrate the accuracy of the developed sensor.

The samples stored at −20 °C in the freezer, were thawed at room temperature. The test tube was filled with 1.0 mL of 1.0 mM COD, 3.6 mL of a serum sample, and 5.4 mL of acetonitrile to make the 0.1 mM serum solution. Afterward, the mixture was centrifuged at 5000 rpm for 20 min. to get precipitation of protein residues. A serum supernatant in a solution of MeOH was used to create the serum calibration curve. A urine sample was taken from healthy individuals, and the preparation of the spiked urine sample was the same as the above serum solution.

3. Results and Dıscussıon

3.1. Characterization of polymeric films

In order to confirm the functional groups of the synthesized material,

the chemical characterization of the developed sensor was studied by using ATR-FTIR spectra measured in the wavenumber range of 4000–650 cm^{-1}. From Fig. 2A, the band at 3404 cm^{-1} is the characteristic band for the polymeric film, which is related to the attribution of –OH stretching. In addition, the band at 2946 cm^{-1} (C–H stretching) and 1724 cm^{-1} (carbonyl stretching vibration of ester groups) are also specific bands that demonstrated the presence of the matrix monomer of HEMA in the sensor material. Otherwise, the characteristic infrared bands of amide I (1640 cm^{-1}), amide II (1551 cm^{-1}), and indole (CC ring, 1599 cm^{-1}) are matched up for functional monomer MA-Trp in the sensor material. Moreover, a comparison of MIP with NIP showed no obvious difference as both NIP and MIP-based polymers contain the same functional monomer, MA-Trp. These results demonstrated that functional monomer was successfully incorporated into the polymeric structures. In addition, morphological analysis of synthesized film produced on the electrode was performed with scanning electron microscopy (SEM), shown in Fig. 2B. The SEM images show that the synthesized sensor surfaces had a rough and porous morphology. It is seen form the images that there is a significant difference in the mophological aspect of MIP and NIP. The image of MIP has more pores and heterogeneous distribution, as expected due to the removal of the template by etching of ZnO nanoparticles.The porous morphology due to the sacrificial pore maker, ZnO, leads to easy accessibility of the template to the recognition sites.

3.2. Electrochemical characterization

Electrochemical characterization techniques describing the charge transfer resistance and electron transfer processes occurring on the electrode surface are evaluated using CV and EIS approaches. The electrochemical behavior of the MA-Trp@MIP/GCE sensor was obtained using 5 mM $[Fe(CN)_6]^{3-/4-}$ at different steps after polymerization, removal, and rebinding. The CV and EIS data for each step of the polymerization process are shown in Fig. 3. The peak intensity of the redox probe achieves its maximum value as shown in Fig. 3A, which belongs to the bare electrode; due to its surface being empty, there are no factors preventing electron transport so the peak current is the highest. After polymerization, the peak density of $[Fe(CN)_6]^{3-/4-}$

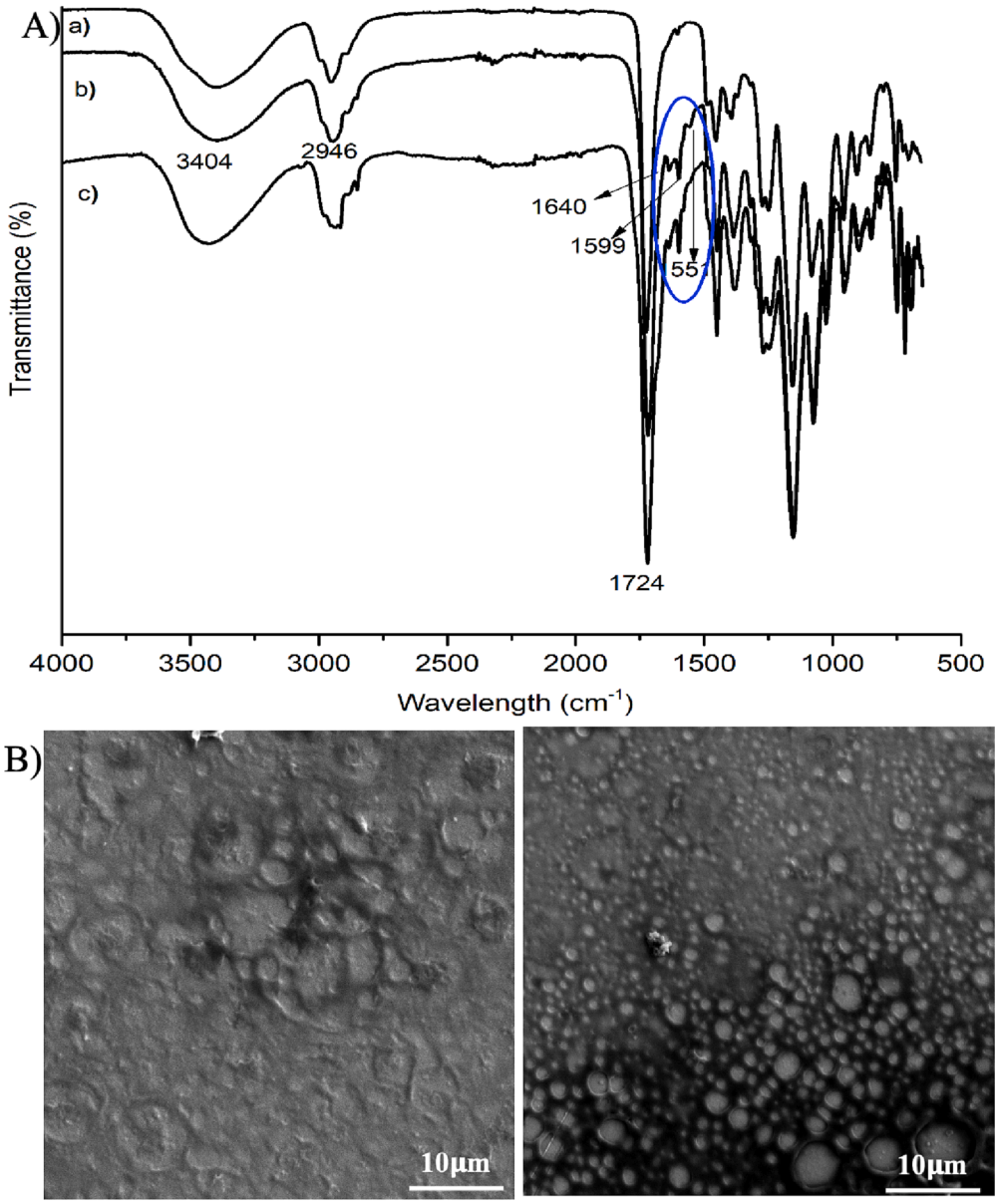


Fig. 2. The characterization of the electrode surface. (A) ATR-FTIR spectra of (a) HEMA, (b) MIP, and (c) NIP surface; (B) SEM images of NIP (left) and MIP surface (right).

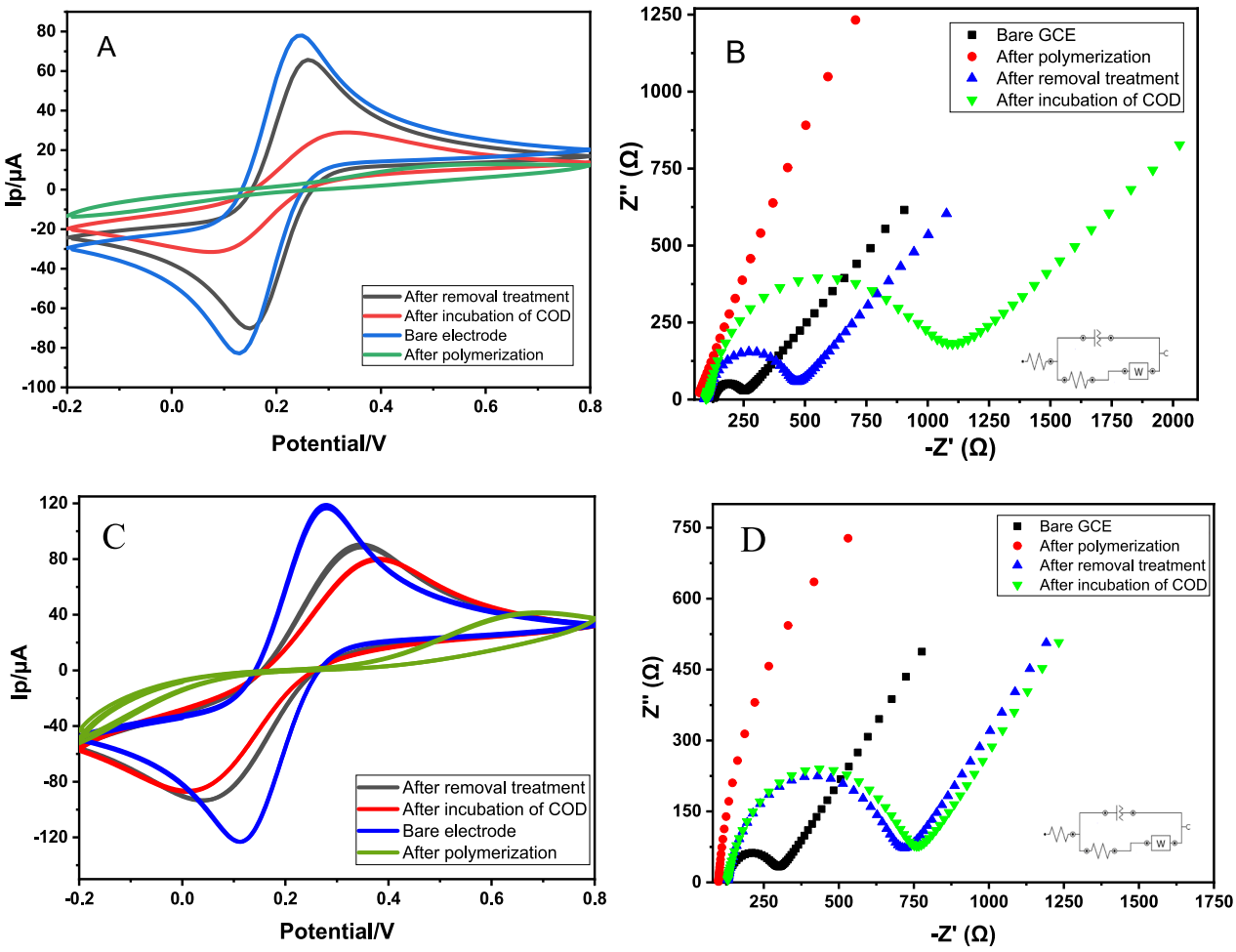


Fig. 3. (A) CV, and (B) EIS measurements for MIP, (C) CV, and (D) EIS measurements for NIP of bare GCE, after polymerization, removal, and after incubation of COD.

disappears since the polymeric film formed on the electrode surface inhibits electron transport. When the COD molecule is removed from the polymeric structure, specific cavities are created, and the peak current of $[Fe(CN)_6]^{3-/4-}$ is lower than bare GCE. With the filling of cavities in certain gaps by rebinding of known concentration of COD, the resulting peaks are smaller than those obtained after removal. EIS measurements were also used to evaluate the same procedures. The results of the EIS measurements are given in Fig. 3B. The Rct value was fairly low since electron transport is possible on the bare GCE surface. (139.2 Ω). The presence of the polymeric coating on the GCE surface after polymerization results in the greatest Rct value (13100), since it hinders electron transit. A decrease in the Rct value (358.54 Ω) was seen after removing the COD molecules. This indicates the formation of cavities on the electrode surface after removal. However, since the Rct value (933.64 Ω) rises after rebinding, it confirms that the COD molecules selectively bind to the cavities found in the polymeric network. In addition, CV and EIS plots were evaluated in the absence of template molecules to confirm the electrochemical characterization of the developed sensor (Fig. 3C and Fig. 3D). While the values after removal and after rebinding in the absence of the template molecule were practically identical, these results demonstrated the accuracy of the NIP-based sensor.

3.3. Optimization parameters

3.3.1. Monomer/template ratio

One of the critical parameters for producing a permanent and efficient polymeric film is the monomer: template ratio. Polymeric film formation is directly related to the interactions between the monomer and the template molecule, so the monomer: template ratio should be optimized. In this regard, in Fig. 4A, the various monomer: template ratios (1:1, 2:1, 3:1, 4:1, and 5:1) were examined by calculating the differences between the peak currents obtained after removal and polymerization, and the optimum ratio was found to be 3:1. Monomer: template ratio may provide stable molecular imprinting processes and increase the sensor selectivity. In contrast, the large mole ratio of the monomer might damage imprinting sites, leading to a nonselective electrochemical response for the template. According to the obtained results, MA-Trp: COD with a ratio of 3:1 was selected as the optimum ratio.

3.3.2. Dropping volume

The amount of the polymerization solution put onto the GCE surface needs to be optimized as it directly affects the thickness of the polymeric film and the polymer formation process. For this reason, a polymerization solution in five different volumes (0.25, 0.5, 0.75, 1.0, and 1.25 μL) was dropped onto the electrode surface and tested (Fig. 4B). By taking the difference of peak current values after removal and polymerization, the optimum dropping amount was found to be 0.5 μL.

3.3.3. Photopolymerization time

The preparation process of the MA-Trp@MIP/GCE sensor was carried out under a UV lamp at 365 nm. The photopolymerization time under a UV lamp must be optimized to form a stable polymeric film on the GCE surface. After dropping 0.5 μL of polymerization solution onto

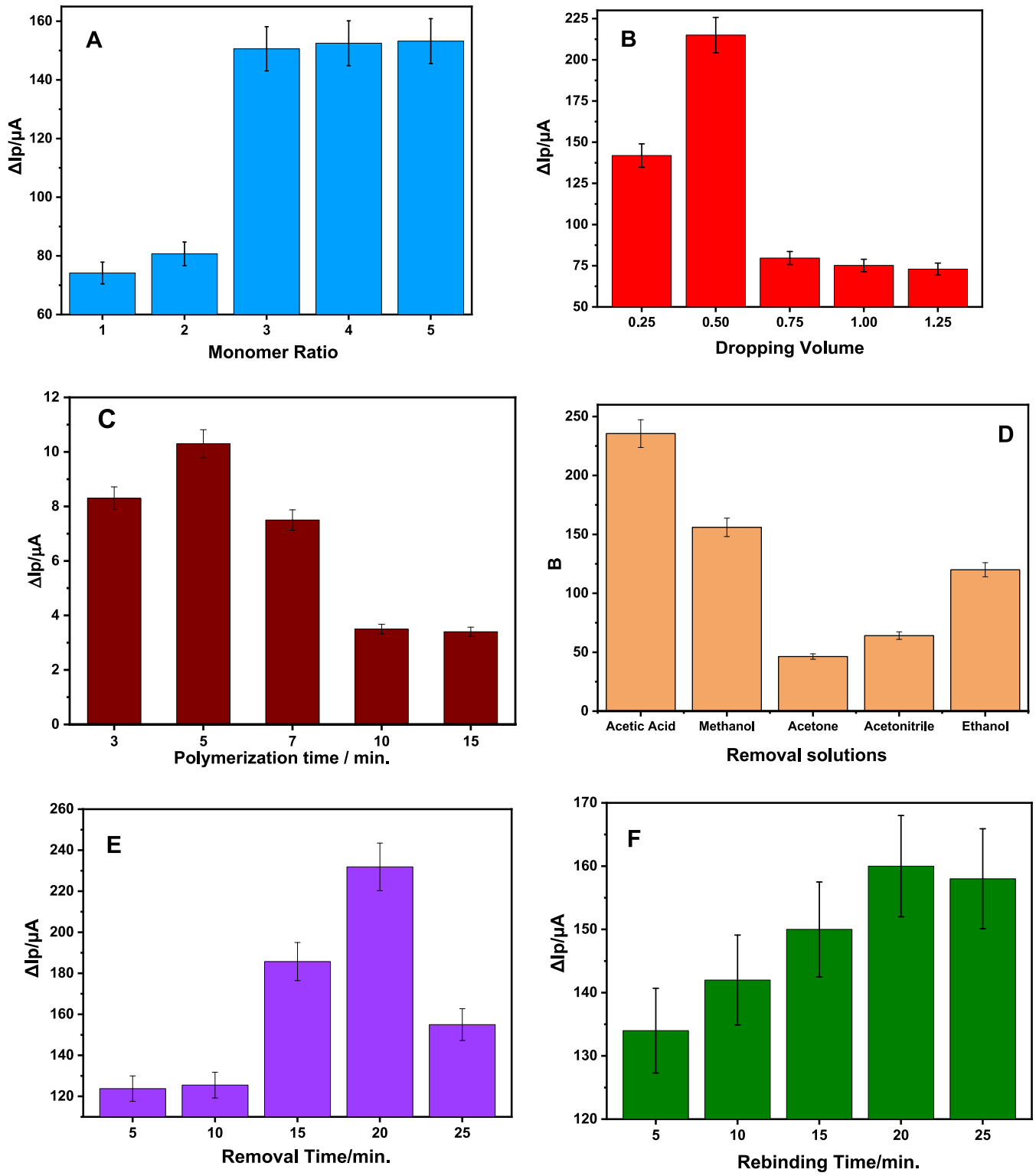


Fig. 4. The plots of ΔIp values of differential pulse voltammograms (A) monomer ratio, (B) dropping volume, (C) photopolymerization time, (D) removal solutions, (E) removal time, and (F) rebinding time.

the electrode surface, it was left under UV light for 3, 5, 7, 10, and 15 min. Then the current values were compared by taking the difference of peak current values after removal and polymerization; the optimal time to create the sensor was determined as 5 min. (Fig. 4C).

3.3.4. *Removal solution and time*

The most crucial stage following the successful formation of MIP films is efficient template removal solution and time. When the template molecule is wholly removed, some recognition sites are created. Thus, the efficient removal of the template is a crucial step in the construction of the MIP sensor. Acetic acid (10 M), MeOH, acetone, acetonitrile, and ethanol were tested to remove the template from the polymeric matrix. Acetic acid is a strong hydrogen bonding solvent [32]. Its effects on the removal process are higher than the other solvents shown in (Fig. 4D),

and it was chosen as the removal solvent. The peak current of the removal solvents was evaluated via the subtraction value of the after removal and polymerization. After selecting the removal solution, the next step is determining the required removal time. Several removal durations between 5 and 25 min were assessed to determine how long the sample was in contact with the acetic acid solution. Fig. 4E demonstrates that the highest peak value was reached at 20 min. Then it started to decrease because of breaking/reforming interpolymeric interactions between polymeric chains, which distorts the imprinted cavities. At the same time, the surface coverage rate/distribution of pores on the electrode surface might be varied during the longer incubation process. Consequently, 20 min was the best value for subsequent studies.

3.3.5. Rebinding time

The template's rebinding process directly impacts the developed sensor's analytical capability and sensor validation. As given in Fig. 4F, at 5×10^{-13} M COD concentration with different incubation periods in the range of 5–20 min were examined to guarantee robust and stable attachment to the specific holes that are exposed following removal. When the subtraction of peak currents following removal and rebinding processes (ΔI) was assessed, it was observed that after 20 min, the particular gaps may have reached saturation, and the ΔI value remains unchanged. As a result, 20 min was decided upon as the optimal rebinding time.

3.4. Analytical performance of developed sensors

The analytical performance of the MA-Trp@MIP/GCE was assessed after incubation of different concentrations of COD with DPV measurements to find a linear working range for COD determination. The calibration graph was created by standard COD solutions in five different concentrations, and the linearity range was obtained in the concentration range of 0.1–1.0 pM. It was discovered that the equation observed, $\Delta I = 6.96 \times 10^{13} \times \text{COD (M)} + 7.02$, $r = 0.999$, respectively represented the linear regression equation and correlation coefficient. The limit of detection (LOD) and the limit of quantification (LOQ) were found at 0.0150 pM and 0.050 pM via applying the mathematical operations as 3.3× and 10.0× standard deviation (s)/slope of the calibration curve (m), for LOD and LOQ, respectively [33]. Some regression parameters are summarized in Table 1. DPV graph of developed sensor responses against different concentrations of COD indicates that when the concentration of rebound COD increases, the current value decreases since the cavities of the polymeric film begin to fill then the current decreases because of an insulating feature of the polymeric layer. The DPV voltammograms of MA-Trp@MIP/GCE with different COD concentrations in standard solution, spiked serum, and urine solution were shown in Fig. 5A, 5C, and 5E, respectively.

The calibration curve of COD with MA-Trp@MIP/GCE and NIP-sensor in standard solution, spiked serum, and urine solution was shown in Fig. 5B, 5D, and 5F, respectively. These figures showing the comparison of the MA-Trp@MIP/GCE and NIP-sensor revealed that the current value gradually increases for the MIP-based sensor, although, it remains almost unchanged for the NIP-based sensor. The results directly depend on the selective cavities created in the presence of the template (COD) and exposed after the removal process. During the rebinding process, the template and polymeric matrix interacted so the current value was significantly changed because the rebounded amounts of COD were varied with respect to its different initial concentrations. In the case of the NIP-based sensor, there are no selective cavities in the polymeric matrix; therefore, no complementary structure was formed to interact with COD molecules. This resulted in the current value remaining almost the same. The prepared sensor was employed repeatedly for measurements throughout the day. It made it possible to perform 10 repeatable measurements to be taken at each stage of the MIP, including after polymerization, after removal, and after rebinding. In addition, the repeatability of the MA-Trp@MIP/GCE sensor was examined for three days. For this, the MIP-modified electrode was kept in a desiccator. The repeatability of the electrode surface was checked and electrode performance was obtained as 92% at the end of the 3rd day.

Fig. S2 shows the effect of ZnO nanoparticles on COD detection with different electrodes. As seen in the results, the maximum ΔIp value was obtained in the presence of ZnO nanoparticles. The ΔIp values obtained for MA-Trp@MIP/GCE and MA-Trp@MIP/GCE (without ZnO) were found to be 255.4 μA and 155.8 μA, respectively. Moreover, ZnO nanoparticles were used as materials that increase the porosity at the interface of the polymeric walls, which increases the current responsiveness. The outcomes demonstrated enhanced accessibility and a stronger current responsiveness in the interface printing film.

Table 1
Regression parameters of COD.

	Standard solution	Serum sample	Urine Samples
Linearity range (pM)	0.1–1.0	0.1–1.0	0.1–1.0
Slope (μA M^{-1})	6.96×10^{13}	8.85×10^{13}	8.53×10^{13}
SE of slope	1.02×10^{12}	3.26×10^{12}	4.89×10^{12}
Intercept (μA)	7.02	13.79	12.39
SE of intercept	0.84	2.00	3.00
Correlation coefficient (*r*)	0.999	0.998	0.995
LOD (pM)	0.0150	0.0193	0.0108
LOQ (pM)	0.0500	0.0644	0.0359
Repeatability of peak current (RSD%)*	0.66	0.88	1.36
Reproducibility of peak current (RSD%)*	1.24	1.69	1.87

*Each value is the mean of five experiments.

3.5. Application of tablet form, spiked serum, and urine samples

The developed sensor's applicability studies were examined in tablet dosage form, spiked serum, and urine samples. The obtained DPV voltammograms and calibration curves of tablet form, spiked serum, and urine samples were given in Fig. 5. All analytical parameters of the tablet, spiked serum, and urine samples were summarized in Table 2. LOD values for the tablet and these biological samples were found as 0.0150 pM, 0.0193 pM, and 0.0108 pM, respectively. Meanwhile, in the same order, LOQ values were calculated as 0.0500 pM, 0.0644 pM, and 0.0359 pM, respectively. In addition, the recovery results for tablet, serum, and urine samples were found as 101.514%, 101.424%, and 98.544%, respectively. These results show that the developed sensor was successfully applied to tablet form, spiked serum, and urine.

3.6. Selectivity studies

The selectivity coefficient (k), which is an essential parameter to assess the MIPs' effectiveness by using structurally and chemically similar compounds such as ethyl morphine (EM), dihydrocodeine (DCOD), trimethoprim (TMP), and dextromethorphan (DMP). The selectivity of the MA-Trp@MIP/GCE sensor was also examined using DPV measurements. The selectivity coefficient (k) was defined as $k = \text{current value}_{\text{template}}/\text{current value}_{\text{competitor}}$ shows that selectivity (k) found for COD was greater; this implies that MIP has relatively better binding tendencies with template COD as compared to other compounds. The relative selectivity coefficient (k') designating the specific recognition properties of the MIPs was estimated by the selectivity coefficient of the COD for MIP/GCE and NIP/GCE, calculated as $k' = k_{MIP}/k_{NIP}$. (Table S3). A high k' value confirmed that the imprinting process was achieved successfully and provided specific recognition sites toward COD based on the size and shape of the template's molecules. According to these values, COD imprinted sensor was 3.78, 3.58, 5.72, and 3.57 times selective with respect to EM, DCOD, TMP, and DMP molecules,

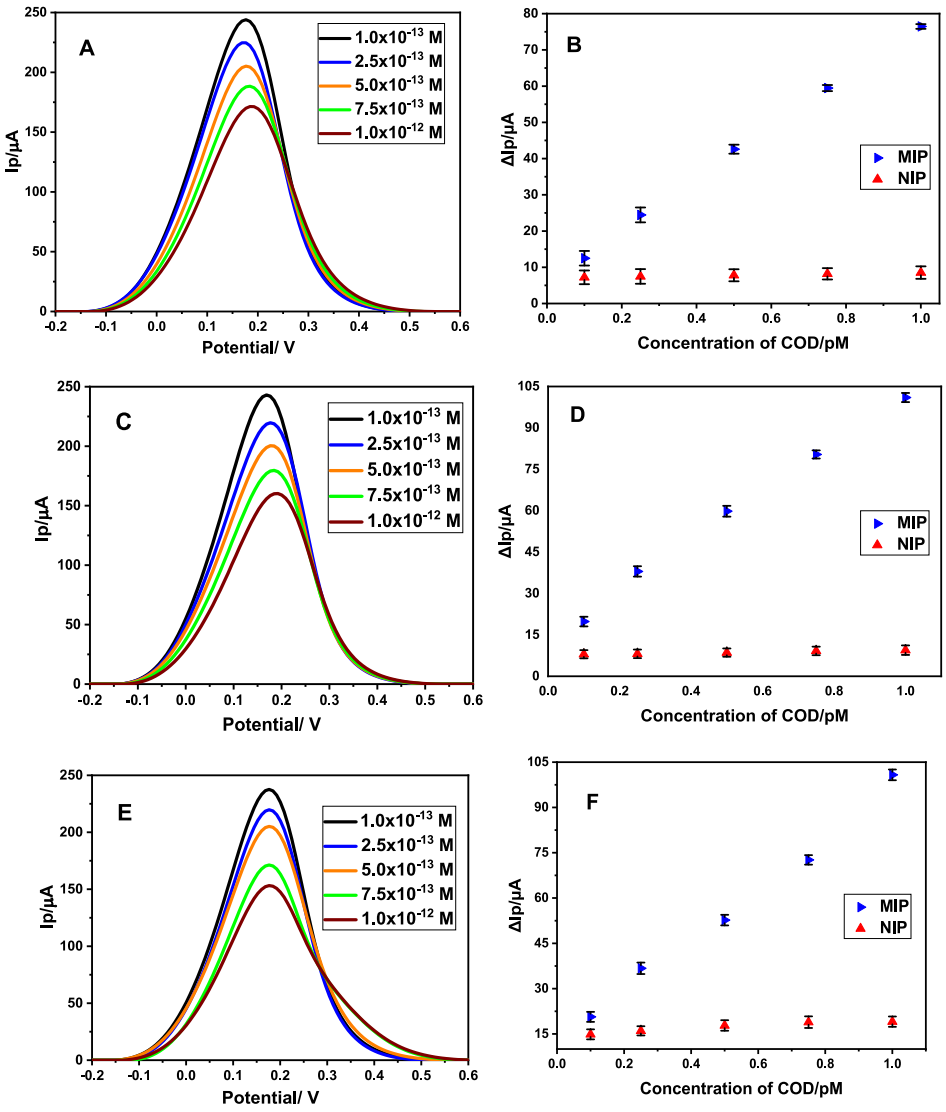


Fig. 5. DPV voltammograms of the MA-Trp@MIP/GCE with COD concentrations (0.10 pM, 0.25 pM, 0.50 pM, 0.75 pM, and 1.0 pM) in (A) standard solution, (C) spiked serum solution, and (E) spiked urine solution. The calibration curve of COD with MA-Trp@MIP/GCE and NIP in (B) standard solution, (D) spiked serum solution, and (F) spiked urine solution.

Table 2
Some analytical parameters of the tablet, spiked serum, and urine samples.

	Tablet dosage form (Apranax®)	Serum sample	Urine samples
Label amount (mg)	30.000	-	-
Found amount (mg)*	30.075	-	-
RSD%*	0.546	-	-
Bias%	0.250	-	-
Spiked amount (mg)	1.000	1.000	1.000
Found amount (mg)*	1.003	1.009	1.013
Average recovery (%)	101.51	101.42	98.54
RSD% of recovery*	0.631	1.488	0.622
Bias%	0.300	0.800	1.300

*Each value is the mean of five experiments.

respectively.

3.7. Interference studies

Besides the selectivity studies against the structurally similar competitors, interference studies were also tested with 5×10^{-13} M COD concentration against possible interfering agents such as K^+, NO_3^-, Na^+, SO_4^{2-}, Mg^{2+}, Cl^-, dopamine (DOP), paracetamol (PAR), uric acid (UA) and ascorbic acid (AA). Although the molar concentration of interfering agents for the selectivity study was 10 times higher than the COD concentration, the peak current of COD did not change significantly. As summarized in Fig. S3, the recovery was calculated between 99.91% and 102.99% whereas the relative standard deviation (RSD) was between 1.09% and 1.70%. According to the results, it was found that the interference agents do not have any effect on the analytical ability of the MA-Trp@MIP/GCE sensor.

3.8. Comparison with related literature

As mentioned before, the most prevalent analgesics on the market are opiates and their derivatives. Due to their addictive effects, it is

possible to encounter undesirable situations including accidents, crimes and endangering society. In this context, there has been a growing demand for analytical methods to simultaneously determine codeine, fentanyl, and morphine over the years [34–36]. Especially, MIP-based electrochemical methods have various benefits over other approaches, including being inexpensive, simple to use, requiring less time for analysis, using non-toxic solvents, eco-friendly electrode modifications, and minimum energy usage. Because of these factors, electrochemical techniques are advantageous for identifying opioid analgesics. For electrochemical sensor methods, different nanomaterials such as single-walled carbon nanotubes, graphene, chitosan, cobalt ferrite, reduced graphene oxide, and hierarchical porous carbon have been used to detect codeine [37–41]. These nanomaterials synthesis routes require extended time, expensive materials, and usage of toxic materials. Additionally, their modification to electrodes causes inconsistent results. For instance, Afkhami et al. [37] synthesized nanocomposite of graphene (Gr) and $CoFe_2O_4$ nanoparticles; as a first step, graphite oxide and then nanocomposite material were synthesized. These synthesis pathways need concentrated acids, explosive material sodium nitrate, and a special atmospheric environment nitrogen atmosphere. After that, the carbon paste electrode was prepared with nanocomposite, graphite powder, and paraffin oil so that the whole process lacked simplicity. Some of these sensors concerning their analytical performances are summarized in Table S4. Regarding detection limit, linear range, and sample applications, it is evident that the generated sensor is comparable to those techniques. This developed method's most crucial comparable feature is its low detection limit.

4. Conclusıon

For the first time, the particular functional monomer based on amino acid, N-methacryloyl-L-tryptophan (MATrp), polymer matrix HEMA, and a pore-making sacrificial material (ZnO) were used to fabricate a molecularly imprinted porous polymeric film-based electrochemical sensor for selective COD detection from tablet and biological samples. The MA-Trp@MIP/GCE sensor shows sensitive and selective determination of COD in spiked serum, urine samples, and tablet samples. The limit of detection (LOD) and dynamic linear working range was calculated as 0.0150 pM and 0.1–1.0 pM, respectively. The proposed electrochemical sensor has shown excellent recovery in human urine, commercial serum samples, and tablet form, with recoveries of 98.544%, 101.424%, and 101.514%, respectively. The electrochemical characterization of MIP-based sensors was confirmed by CV and EIS techniques. The created MIP sensor showed excellent analytical ability with high selectivity, interference resistance, good accuracy, and precision results, offering analytical analysis in the pharmaceutical industry.

CRediT authorship contribution statement

Merve Yence: Investigation, Conceptualization, Writing – original draft. **Ahmet Cetinkaya:** Investigation, Conceptualization, Writing – original draft. **Mehmet Emin Çorman:** Investigation, Conceptualization, Writing – original draft. **Lokman Uzun:** Investigation, Conceptualization, Writing – original draft. **Mehmet Gokhan Caglayan:** Supervision, Conceptualization, Writing – review & editing. **Sibel A. Ozkan:** Supervision, Conceptualization, Writing – review & editing.

Declaration of Competing Interest

The authors declare that they have no known competing financial interests or personal relationships that could have appeared to influence the work reported in this paper.

Data availability

Data will be made available on request.

Acknowledgement

This work was produced as a part of Merve Yence's Ph.D. thesis. Merve Yence thanks the financial support from the Technological Research Council of Turkiye (TUBITAK) under the BIDEB/2211-A Ph.D. Scholarship Programmes and ARDEB/1004 Ph.D. Scholarship Programmes. Ahmet Cetinkaya thanks the financial support from the Council of Higher Education 100/2000 (YOK) under the special 100/2000, the TUBITAK under the BIDEB/2211-A Ph.D. Scholarship Programmes and ARDEB/1004 Ph.D. Scholarship Programmes.

Appendix A. Supplementary data

Supplementary data to this article can be found online at https://doi.org/10.1016/j.cej.2023.144765.

References

[1] J. Kirchheiner, H. Schmidt, M. Tzvetkov, J.-T. Keulen, J. Lötsch, I. Roots, J. Brockmöller, Pharmacokinetics of codeine and its metabolite morphine in ultra-rapid metabolizers due to CYP2D6 duplication, Pharmacogenomics J. 7 (2007) 257–265, https://doi.org/10.1038/sj.tpj.6500406.
[2] L. Yip, B. Mégarbane, S.W. Borron, Opioids, in: Haddad Winchester's Clin. Manag. Poisoning Drug Overdose, Elsevier, 2007: pp. 635–658. doi: 10.1016/B978-0-7216-0693-4.50038-4.
[3] N.G. Bowery, Codeine, in: XPharm Compr. Pharmacol. Ref., Elsevier, 2007: pp. 1–4. https://doi.org/10.1016/B978-008055232-3.61504-1.
[4] H. Malm, C. Borisch, Analgesics, non-steroidal anti-inflammatory drugs (NSAIDs), muscle relaxants, and antigout medications, in: Drugs Dur. Pregnancy Lact., Elsevier, 2015: pp. 27–58. https://doi.org/10.1016/B978-0-12-408078-2.00002-0.
[5] M. Yence, A. Cetinkaya, S.I. Kaya, S.A. Ozkan, Recent Developments in the Sensitive Electrochemical Assay of Common Opioid Drugs, Crit. Rev. Anal. Chem. (2022) 1–14, https://doi.org/10.1080/10408347.2022.2099732.
[6] H. Laycock, C. Bantel, Opioid mechanisms and opioid drugs, Anaesth. Intensive Care Med. 20 (2019) 450–455, https://doi.org/10.1016/j.mpaic.2019.05.009.
[7] I. Boureima Mahamane, S.I. Kaftanoglu, M.G. Caglayan, Fluorescence detection of ethylmorphine through terbium complex, Spectrosc. Lett. 53 (2020) 523–528, https://doi.org/10.1080/00387010.2020.1792501.
[8] R.E. Akhigbe, O.S. Ebiwonjumi, L.O. Ajayi, A.F. Ajayi, Codeine alters female reproductive function by targeting ovarian steroidogenesis and folliculogenesis via the induction of oxidative stress, inflammation, and apoptosis, Reprod. Toxicol. 109 (2022) 1–9, https://doi.org/10.1016/j.reprotox.2022.02.001.
[9] J. Reno, M. Lou Leary, M. Mccoy Roberts, Drug Testing in a Drug Court Environment: COMMON ISSUES TO ADDRESS, Drug Court, Resour. Ser. (2000). https://www.ncjrs.gov/pdffiles1/ojp/181103.pdf.
[10] Ç. Karakükcü, M.Z. Çıracı, D. Kocer, M.Y. Faydalı, M.A. Serdar, Evaluation of optimal urine screening and confirmation cut-off values for opiates, at a national reference laboratory, Turkish, J. Biochem. 46 (2021) 593–602, https://doi.org/10.1515/tjb-2020-0614.
[11] H. Abdolmohammad-Zadeh, A. Zamani, Z. Shamsi, Preconcentration of morphine and codeine using a magnetite/reduced graphene oxide/silver nano-composite and their determination by high-performance liquid chromatography, J. Chromatogr. A 1590 (2019) 2–9, https://doi.org/10.1016/j.chroma.2018.12.064.
[12] B. Weingarten, H.-Y. Wang, D.M. Roberts, Determination of codeine in human plasma by high-performance liquid chromatography with fluorescence detection, J. Chromatogr. A 696 (1995) 83–92, https://doi.org/10.1016/0021-9673(94)01212-W.
[13] C.P.W.G.M. Verwey-Van Wissen, P.M. Koopman-Kimenai, T.B. Vree, Direct determination of codeine, norcodeine, morphine and normorphine with their corresponding O-glucuronide conjugates by high-performance liquid chromatography with electrochemical detection, J. Chromatogr. B Biomed. Sci. Appl. 570 (1991) 309–320, https://doi.org/10.1016/0378-4347(91)80534-J.
[14] M. Moller, K. Aleksa, P. Walasek, T. Karaskov, G. Koren, Solid-phase microextraction for the detection of codeine, morphine and 6-monoacetylmorphine in human hair by gas chromatography–mass spectrometry, Forensic Sci. Int. 196 (2010) 64–69, https://doi.org/10.1016/j.forsciint.2009.12.046.
[15] A. Lodha, A. Pandya, P.G. Sutariya, S.K. Menon, A smart and rapid colorimetric method for the detection of codeine sulphate, using unmodified gold nanoprobe, RSC Adv. 4 (2014) 50443–50448, https://doi.org/10.1039/C4RA06269H.
[16] V. Rana, M.V. Cañamares, T. Kubic, M. Leona, J.R. Lombardi, Surface-enhanced Raman Spectroscopy for Trace Identification of Controlled Substances: Morphine, Codeine, and Hydrocodone, J. Forensic Sci. 56 (2011) 200–207, https://doi.org/10.1111/j.1556-4029.2010.01562.x.
[17] L. Wu, H. Yan, G. Li, X. Xu, L. Zhu, X. Chen, J. Wang, Surface-imprinted gold nanoparticle-based surface-enhanced raman scattering for sensitive and specific

detection of patulin in food samples, Food Anal. Methods. 12 (2019) 1648–1657, https://doi.org/10.1007/s12161-019-01498-4.
[18] G. Vasapollo, R. Del Sole, L. Mergola, M.R. Lazzoi, A. Scardino, S. Scorrano, G. Mele, Molecularly imprinted polymers: present and future prospective, Int. J. Mol. Sci. 12 (2011) 5908–5945, https://doi.org/10.3390/ijms12095908.
[19] B. Wang, J. Hong, C. Liu, L. Zhu, L. Jiang, An electrochemical molecularly imprinted polymer sensor for rapid β-lactoglobulin detection, Sensors 21 (2021) 8240, https://doi.org/10.3390/s21248240.
[20] S. Wang, C. Wang, Y. Xin, Q. Li, W. Liu, Core–shell nanocomposite of flower-like molybdenum disulfide nanospheres and molecularly imprinted polymers for electrochemical detection of anti COVID-19 drug favipiravir in biological samples, Microchim. Acta 189 (2022) 125, https://doi.org/10.1007/s00604-022-05213-9.
[21] M.E. Çorman, A. Cetinkaya, C. Armutcu, E. Bellur Atici, L. Uzun, S.A. Ozkan, A sensitive and selective electrochemical sensor based on molecularly imprinted polymer for the assay of teriflunomide, Talanta 249 (2022), 123689, https://doi.org/10.1016/j.talanta.2022.123689.
[22] A. Cetinkaya, S.I. Kaya, M.E. Çorman, M. Karakaya, E. Bellur Atici, S.A. Ozkan, A highly sensitive and selective electrochemical sensor based on computer-aided design of molecularly imprinted polymer for the determination of leflunomide, Microchem. J. 179 (2022), 107496, https://doi.org/10.1016/j.microc.2022.107496.
[23] A.A. Hasseb, N.D.T. Abdel Ghani, O.R. Shehab, R.M. El Nashar, Application of molecularly imprinted polymers for electrochemical detection of some important biomedical markers and pathogens, Curr. Opin. Electrochem. 31 (2022) 100848.
[24] A. Dinu, C. Apetrei, A review of sensors and biosensors modified with conducting polymers and molecularly imprinted polymers used in electrochemical detection of amino acids: phenylalanine, tyrosine, and tryptophan, Int. J. Mol. Sci. 23 (2022) 1218, https://doi.org/10.3390/ijms23031218.
[25] A. Motaharian, F. Motaharian, K. Abnous, M.R.M. Hosseini, M. Hassanzadeh-Khayyat, Molecularly imprinted polymer nanoparticles-based electrochemical sensor for determination of diazinon pesticide in well water and apple fruit samples, Anal. Bioanal. Chem. 408 (2016) 6769–6779, https://doi.org/10.1007/s00216-016-9802-7.
[26] D. Udomsap, H. Brisset, G. Culioli, P. Dollet, K. Laatikainen, H. Siren, C. Branger, Electrochemical molecularly imprinted polymers as material for pollutant detection, Mater. Today Commun. 17 (2018) 458–465, https://doi.org/10.1016/j.mtcomm.2018.10.019.
[27] M.E. Çorman, A. Cetinkaya, G. Ozcelikay, E. Özgür, E.B. Atici, L. Uzun, S.A. Ozkan, A porous molecularly imprinted nanofilm for selective and sensitive sensing of an anticancer drug ruxolitinib, Anal. Chim. Acta. 1187 (2021), 339143, https://doi.org/10.1016/j.aca.2021.339143.
[28] E.I. Paruli, O. Soppera, K. Haupt, C. Gonzato, Photopolymerization and Photostructuring of Molecularly Imprinted Polymers, ACS Appl. Polym. Mater. 3 (2021) 4769–4790, https://doi.org/10.1021/acsapm.1c00661.
[29] J. Zhang, S. Wang, M. Xu, Y. Wang, B. Zhu, S. Zhang, W. Huang, S. Wu, Hierarchically porous ZnO architectures for gas sensor application, Cryst. Growth Des. 9 (2009) 3532–3537, https://doi.org/10.1021/cg900269a.
[30] C. Armutcu, E. Özgür, M.E. Çorman, L. Uzun, Interface imprinted polymers with well-oriented recognition sites for selective purification of hemoglobin, Colloids Surfaces B Biointerfaces. 197 (2021), 111435, https://doi.org/10.1016/j.colsurfb.2020.111435.
[31] D. Hur, S. Ekti, R. Say, N-Acylbenzotriazole Mediated Synthesis of Some Methacrylamido Amino Acids, Lett. Org. Chem. 4 (2007) 585–587, https://doi.org/10.2174/157017807782795556.
[32] A.A. Ensafi, N. Kazemifard, Z. Saberi Dehkordi, Parameters that affect molecular imprinting polymers, in: Mol. Imprinted Polym. Compos., Elsevier, 2021: pp. 21–48. doi: 10.1016/B978-0-12-819952-7.00010-X.
[33] S.A. Ozkan, J.-M. Kauffmann, P. Zuman, Electroanalytical Method Validationmethod validation in Pharmaceutical Analysis and Their Applications, in: 2015: pp. 235–266. doi: 10.1007/978-3-662-47138-8_8.
[34] A.H. Schmidt, Validated HPLC method for the determination of residues of acetaminophen, caffeine, and codeine phosphate on swabs collected from pharmaceutical manufacturing equipment in support of cleaning validation, J. Liq. Chromatogr. Relat. Technol. 29 (2006) 1663–1673, https://doi.org/10.1080/10826070600678381.
[35] M. Freiermuth, J.-C. Plasse, Determination of morphine and codeine in plasma by HPLC following solid phase extraction, J. Pharm. Biomed. Anal. 15 (1997) 759–764, https://doi.org/10.1016/S0731-7085(96)01911-5.
[36] M.E. El-Kommos, K.M. Emara, Determination of phenyltoloxamine salicylamide, caffeine, paracetamol, codeine and phenacetin by HPLC, Talanta 36 (1989) 678–679, https://doi.org/10.1016/0039-9140(89)80263-2.
[37] A. Afkhami, H. Khoshsafar, H. Bagheri, T. Madrakian, Facile simultaneous electrochemical determination of codeine and acetaminophen in pharmaceutical samples and biological fluids by graphene-CoFe2O4 nancomposite modified carbon paste electrode, Sensors Actuators, B Chem. 203 (2014) 909–918, https://doi.org/10.1016/j.snb.2014.07.031.
[38] B. Habibi, M. Abazari, M.H. Pournaghi-Azar, Simultaneous determination of codeine and caffeine using single-walled carbon nanotubes modified carbon-ceramic electrode, Colloids Surfaces B Biointerfaces 114 (2014) 89–95, https://doi.org/10.1016/j.colsurfb.2013.09.026.
[39] Y. Li, K. Li, G. Song, J. Liu, K. Zhang, B. Ye, Electrochemical behavior of codeine and its sensitive determination on graphene-based modified electrode, Sensors Actuators, B Chem. 182 (2013) 401–407, https://doi.org/10.1016/j.snb.2013.03.023.
[40] N. Mohammadi, M. Bahmaei, A.M. Sharif, Highly sensitive CuZnO-Fe3O4/rGO modified glassy carbon electrode for the electrochemical determination of acetaminophen, tyrosine and codeine in human blood plasma and urine, J. Electroanal. Chem. 902 (2021) 115768.
[41] A. Wong, A.C. Riojas, A.M. Baena-Moncada, M.D.P.T. Sotomayor, A new electrochemical platform based on carbon black paste electrode modified with α-cyclodextrin and hierarchical porous carbon used for the simultaneous determination of dipyrone and codeine, Microchem. J. 164 (2021) 106032.